PCCP

Accepted Manuscript


This is an *Accepted Manuscript*, which has been through the Royal Society of Chemistry peer review process and has been accepted for publication.

*Accepted Manuscripts* are published online shortly after acceptance, before technical editing, formatting and proof reading. Using this free service, authors can make their results available to the community, in citable form, before we publish the edited article. We will replace this *Accepted Manuscript* with the edited and formatted *Advance Article* as soon as it is available.

You can find more information about *Accepted Manuscripts* in the Information for Authors.

Please note that technical editing may introduce minor changes to the text and/or graphics, which may alter content. The journal's standard Terms & Conditions and the Ethical guidelines still apply. In no event shall the Royal Society of Chemistry be held responsible for any errors or omissions in this *Accepted Manuscript* or any consequences arising from the use of any information it contains.

ROYAL SOCIETY OF CHEMISTRY

www.rsc.org/pccp

ARTICLE TYPE www. rsc.org/xxxxxx | XXXXXXXX

# Structural instabilities and wrinkles at the grain boundaries in 2-D h-BN: a first-principles analysis

**Anjali Singh and Umesh V. Waghmare***

***Received Xth XXXXXXXXXX 20XX, Accepted Xth XXXXXXXXX 20XX***
***First published on the web Xth XXXXXXXXXX 200X***
**DOI: 10.1039/b000000x**

The structure of grain boundaries (GBs) or interfaces between nano-forms of carbon determines their evolution into 3-D forms with nano-scale architecture. Here, we present a general framework for the construction of interfaces in 2-D h-BN and graphene in terms of (a) stacking faults and (b) growth faults, using first-principles density functional theoretical analysis. Such interfaces or GBs involve deviation from their ideal hexagonal lattice structure. We show that a stacking fault involves a linkage of rhombal and octagonal rings (4:8), and a growth fault involves a linkage of paired pentagonal and octagonal rings (5:5:8). While a growth fault is energetically more stable than a stacking fault in graphene, the polarity of B and N leads to the reversal in their relative stability in h-BN. We show that the planar structure of these interfacing grains exhibits instability with respect to buckling (out-of-plane deformation), which results in the formation of a wrinkle at the grain boundary (GB) and rippling of the structure. Our analysis leads to prediction of new types of low-energy GBs of 2-D h-BN and graphene. Our results for electronic and vibrational signatures of these interfaces and an STM image of the most stable interface will facilitate their experimental characterization, particularly of the wrinkles forming spontaneously at these interfaces.

**Keywords:** graphene, h-BN, interfaces, spectroscopic signatures, electronic structure, grain boundary

## 1 Introduction

Fascinating properties of 0-D, 1-D and 2-D nano-forms of carbon have generated immense activity of research in the last two decades.[1–3] Among these, graphene (the 2-D form) is the mother form, which gives rise to other nano-forms through deformation or introduction of structural point defects (involving pentagonal carbon rings). Of late, there have been efforts to develop 3-D *nano*-structured forms of carbon that would open up new domains of applications.[4,5] To this end, understanding of the structure of interfaces or extended line defects in graphene is expected to be crucial. While 2-D h-BN is the only other known material which is isostructural to graphene (almost lattice matched!), it exhibits rather different structural defects.[6] As a result, a solid solution, $C_x(BN)_{1-x}$ (CBN) between h-BN and graphene is promising in the development and engineering of 3-D materials with nano-scale architecture based on h-BN and graphene.[7] To develop such 3-D nano-forms of CBN, it is important to understand the interfaces or GBs in h-BN and graphene on the same footing. Such interfaces are analogous to GBs (well known in the context of 3-D crystalline materials), as they determine the way in which two flakes (grains) of 2-D materials are stitched together through non-hexagonal structural units (*e.g.* pentagon and heptagon pair[8]). In this work, we use the terms 'interfaces' and 'line defects' to broadly represent GBs.

Line and point defects invariably occur during the synthesis of these materials. They alter the local structural symmetry and can have interesting effects on their global properties, such as band gaps of h-BN.[9] Graphene and h-BN can be synthesized *via* different techniques such as chemical vapor deposition (CVD), chemical exfoliation, and electrochemical reduction.[10–15] The presence of point defects[16–18] and line defects[17,19,20] in h-BN and graphene is clearly evident in detailed characterization based on transmission electron microscopy (TEM) and scanning tunneling microscopy (STM). Notable changes in electronic,[21–27] mechanical,[28,29] chemical[30] and magnetic[31] properties of graphene have been reported due to such structural changes at the GBs, though only a few reports are available on the analysis of GBs in h-BN and their effects on its electronic[32] and magnetic[33] properties.

Liu *et al.*[33] have discussed dislocations and GBs in monolayered h-BN, analysing square-octagon and pentagon-heptagon pair dislocations and transformation reaction of GBs for the tilt angle varying from 0° to 240°. Their work focused on relative stability and electronic properties of these GBs. Li *et al.*[9] have studied '$B_2$, $N_2$ and $C_2$ pentagon-octagon-

*Theoretical Sciences Unit, Jawaharlal Nehru Centre for Advanced Scientific Research, Jakkur, Bangalore 560 064, India. E-mail: waghmare@jncasr.ac.in*

This journal is © The Royal Society of Chemistry [year]



Physical Chemistry Chemical Physics Accepted Manuscript

pentagon (5-8-5)' line defects in 2D h-BN, and explained electronic and magnetic properties associated with these defects in h-BN. While the structural instabilities are associated with Stone-Wales point defects[22] and line defects[34–36] are known to give rise to buckling of the structure of graphene, analysis of the structural instabilities associated with GBs or line defects in 2D h-BN is lacking. Though Raman spectroscopic characterization of defects in graphene has been quite effective, it lacks the specificity with respect to the kind of defects which requires the identification of specific vibrational signatures (if any) of GBs. It is thus desirable to study structural stability and spectroscopic properties of GBs in monolayer h-BN and graphene in detail.

We present here a detailed structural analysis of extended line defects or GBs in h-BN and graphene benefiting from the ideas of growth and stacking faults that are well established in metallurgy. This is expected to help understand how these GB structures may form during growth of these materials in experiments. The defect structures discussed in this article are essentially 60° GBs[36,37] and inversion domain boundaries[38].

We identify the signatures of these GBs in the electronic and vibrational spectra. Our comparative analysis based on first-principles density functional theoretical (DFT) calculations provide a unified understanding of the interfaces or GB structures in h-BN and graphene. Our systematic scheme for the construction of GBs in these 2-D materials allows us to predict novel low energy interfaces. From their energetics, we assess the relative stability of various GBs in these materials, and understand it in terms of the changes in bonding. The structural instabilities and buckling (ripples and wrinkles) of planar structures associated with these GBs are analysed through a detailed study of their vibrational spectra. The spectroscopic signatures identified here would permit non-invasive characterization of such interfaces using Raman and IR spectroscopies.

## 2 Computational methods

Our first-principles simulations are within the framework of density functional theory (DFT) as implemented in QUANTUM ESPRESSO (QE) package,[39] which employs plane wave basis and pseudopotentials. We use a generalized gradient approximation (GGA) of the Perdew, Burke and Ernzerhof (PBE)[40] form of the exchange correlation energy functional and ultrasoft pseudopotentials[41] to represent the interaction between ionic cores and valence electrons. The plane wave basis for representation of Kohn-Sham wavefunctions and charge density has been truncated with energy cutoffs of 30 Ry and 180 Ry respectively. We aided the convergence to self-consistency by smearing the occupation numbers with the Fermi-Dirac distribution function, with the smearing width of 0.003 Ry. Structures have been relaxed through the minimization of energy using Broyden-Fletcher-Goldfarb-Shenno (BFGS) scheme, until magnitude of each component of Hellman-Feynman force is smaller than 0.001 Ry/bohr. We use a periodic supercell to model 2-D h-BN (monolayer) and graphene. In order to ensure negligible interaction between the nearest periodic images of the 2-D sheet, a vacuum of 15 Å is introduced along c-axis. Integrations over the Brillouin zone are sampled with a 4x3x1 uniform mesh of k-points for a 3x4 supercell (rectangular supercell with 96 atoms, where unit cell consist of 8 atoms) and a 2x6x1 mesh for a 7x2 (rectangular supercell with 104 atoms, where unit cell consists of 8 atoms) supercell for 4:8 and 5:5:8 GBs respectively. Vibrational spectrum at the zone center Γ-point is determined using the frozen-phonon method with finite difference formulae and atomic displacements of ± 0.04 Å.

To assess relative stability of GBs, we define their energy per unit length as:

$$E_{GB} = \frac{E^{GB}_{BN/g} - N \times E_{bulk}}{l} \quad (1)$$

where, $E^{GB}_{BN/g}$ is the total energy of h-BN or graphene supercell with a GB, $E_{bulk}$ is the total energy of a primitive cell of h-BN or graphene, and $N$ is the number of B-N or C-C atomic pairs in the supercell, and $l$ is the length of a GB contained within supercell.

## 3 Results and discussion

### 3.1 Structure and energetics

In this section, we present detailed atomic structure of interfaces in 2-D lattices. There are many ways to construct interfaces[9,21,32,33] which are classified into two types: (i) a stacking fault, in which a semi-infinite half of the 2-D lattice is in misregistry with the other half, and (ii) a growth fault, which is associated with removal of a line of atoms (missed during the growth of the lattice), as reported earlier for graphene[21]. They are essentially the inversion domain boundaries and 60° GBs. The construction of their structure in h-BN and graphene, is discussed below.

**3.1.1 Stacking fault.** A pure h-BN lattice with armchair edges along $\vec{a}$ or $\hat{x}$ is divided into two semi-infinite sheets by a slip line (see Fig. 1a) parallel to $\vec{a}$. A misregistry (or slip) vector, $\vec{v} = 1.5b\hat{x}$ (where, $b$ = bond length) gives a displacement of the upper half of the sheet with respect to the lower half. With introduction of this fault, the neighbouring atoms across the GB form homopolar (B-B and N-N) bonds, which are chemically and energetically not favourable (Fig. 1b). Hence, a 180° rotation of the upper half lattice around the y-axis ('twist') (Fig. 1c) is performed, so that the bonds across the GB line are heteropolar (B-N) and energetically


This journal is © The Royal Society of Chemistry [year]

Physical Chemistry Chemical Physics Accepted Manuscript

more favourable.[42] As a result, a pair of one rectangular (B-N-B-N) ring and one octagonal ring forms, and this structure is labelled as a '4:8' GB. Because of the periodic boundary conditions, two such 4:8 GBs are generated, one at the center of the periodic supercell and another at its edge. Recently, a similar GB has been reported theoretically,[33] in which 4:8 GB is created when two asymmetrical grains join with tilt angles of $0^\circ$, $120^\circ$ and $240^\circ$. However, the resulting atomistic structural

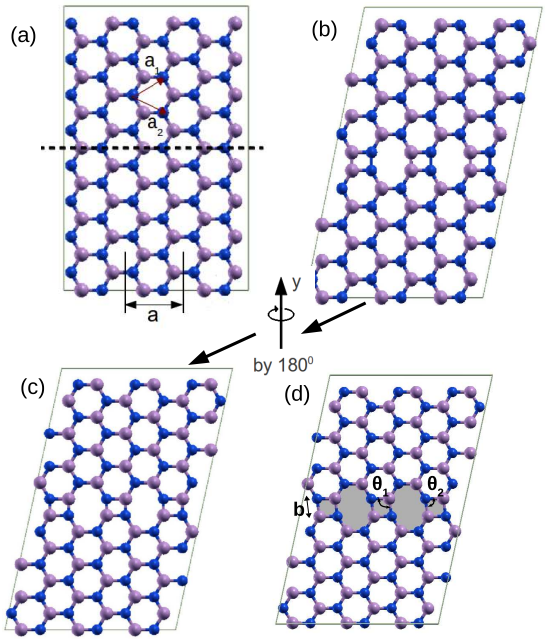


**Fig. 1** Construction of 4:8 GB in h-BN (a) Pure BN lattice (pristine) (b) BN lattice with stacking fault (c) BN lattice with GB twisting and (d) Ground state structure of BN with 4:8 GB (grey shadow shows the GB with octagons and rhombii). The bond length (b) and angles ∠NBN ($\theta_1$) and ∠ BNB ($\theta_2$) are 1.45Å, $98^\circ$ and $82^\circ$ respectively after relaxation. Boron (B) atoms are shown in pink and nitrogen (N) in blue.

changes at the GB have not been discussed. We present a detailed account of how its structure and energetics evolve upon relaxation. We find that the structure at the interface evolves to interlinked rhombal and irregular octagonal rings, whose opposite sides are equal. The B-N bonds elongate from 1.44 Å (bulk h-BN) to 1.46 Å (perpendicular to GB). The bond angles $\theta_1$ and $\theta_2$ of rhombii are $82^\circ$ and $98^\circ$ respectively as shown in Fig. 1d. The stress on the system is zero (after complete structural relaxation) for a defect concentration of 0.2/Å (no. of GB per supercell/distance between two GBs). Stretching of bonds perpendicular to the GBs causes a slight compression of hexagonal rings in the perfect honeycomb region connecting two GBs. The calculated energy of the 4:8 GB is 0.48 eV/Å, in good agreement with earlier estimates (0.4-0.5 eV/Å[33]).

Similarly, the 4:8 GB in graphene is introduced with a misregistry vector $\vec{v} = 1.5b\hat{x}$, which has energy of 0.74 eV/Å for defect concentration of 0.2/Å. Upon structural relaxation, we find that bond angles $\theta_1$ and $\theta_2$ are of $90^\circ$ but the C-C bond perpendicular to the GB weakens from 1.42 Å (in pristine graphene) to 1.47 Å. As a result, we get interlinked rectangular and irregular octagonal rings at the interface. The 4:8 GB is more stable in h-BN than in graphene because the heteroelemental sub-lattices facilitate formation of stable bonds at the interface (which comes from the twist of a grain) in contrast to those in graphene.

**3.1.2 Growth fault.** In construction of a growth fault, we consider two grains of a pure h-BN lattice obtained by cutting across a dashed line along zigzag direction as shown in Fig. 2a, where grains or flakes are marked as 1 and 2. The two grains are anti-symmetric across the dashed line. In grain 2, each B atom is replaced by N atom and N atom is replaced by B atom, such that a symmetric grains with the same polar edges facing each other (Fig. 2b). To introduce a growth fault, we (i) move grain 1 along x-direction such that boron atoms at the edges of the two grains overlap along the dashed line, and (ii) remove one set of boron atoms on this line. This results in a linear chain of rhombii (Fig. 2c) at the interface with B atoms occupying sites at the GB. We ensure equal number of B and N atoms in the supercell, by removing a line of N atoms from the edge of the supercell. Because of the periodic boundary conditions, another GB is thus generated at the boundary of the supercell involving a chain of rhombii with N atoms occupying sites at the GB (Fig. 2d). The relaxation of this structure leads to the formation of a pair of two irregular pentagonal rings with apex angles of $111^\circ$ and one irregular octagonal (with opposite sides of equal length) rings at the GB (Fig. 2e). Thus, we label this as a '5:5:8' GB.

The interfaces with N-N and B-B bonds along the GB will be referred to as '5:5:8 N-N' and '5:5:8 B-B' GBs respectively. While the GB at the edge of the supercell is naively expected to transform into a 5:5:8 B-B GB, it retains its initial structure with rhombii (Fig. 2f), confirming the feasibility of its occurrence in h-BN at 0 K. We label this GB constituted purely of rhombii as a '4:4' GB. This GB transforms into 5:5:8 B-B GB at 1000 K as discussed theoretically by X. Li *et al.*.[9] Along the line of 4:4 GB at the boundary, N-atoms are coordinated with four B-atoms saturating all its valence electrons (energetically favourable), in contrast to B-atoms coordinated with four N-atoms at the center of supercell. Hence, 4:4 GB with B atoms at GB transforms into N-N dimer along the GB (see Fig. 2e). To determine energy of each of these GBs, we simulated BN ribbons containing these GBs at the center running along the length. From these simulations, the estimates of energies of the 5:5:8 N-N and 4:4 GBs in h-BN are 0.77 eV/Å and 1.87 eV/Å respectively. To determine energy of a

Physical Chemistry Chemical Physics Accepted Manuscript

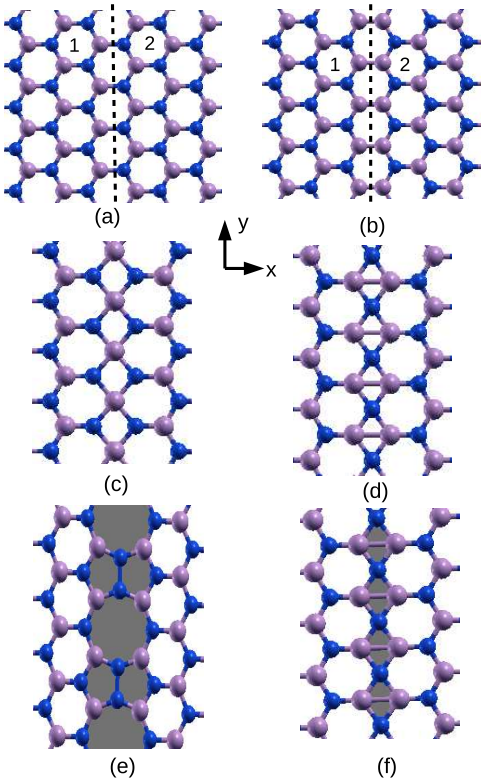


**Fig. 2** Construction of growth fault in h-BN (a) Pure BN lattice (pristine) which can be thought as two grains are connected perfectly along the dashed line (symmetrical grain boundaries with opposite polarity grains). Grain 1 and grain 2 are marked by 1 and 2. (b) Grain 2 is rotated by 180° along z-axis (tilt) with respect to grain 1 such that B-B bond forms perpendicular to dashe d line (symmetrical grain boundaries with same polarity grains). (c) Grain 1 is moved along x-direction such that boron atoms perpendicular to dashed line overlap with each other (one layer of boron atoms is removed). A defect created at the GBs before relaxation (at the center of supercell) (d) Chain of rhombii, GB generated at the edge of the supercell (before relaxation). GBs are marked in shadow in (e) and (f), which show structural modifications after relaxation. Boron (B) atoms are shown in pink and nitrogen (N) in blue.

5:5:8 B-B GB, we interchange the B atoms and the N atoms in the 5:5:8 N-N structure. The calculated energy of the 5:5:8 B-B GB is 0.65 eV/Å, from which it is clear that the 5:5:8 B-B GB is more stable than the other two (5:5:8 N-N and 4:4) GBs in h-BN.

Similarly, a 5:5:8 GB can be created in graphene by the introduction of a growth fault.[21] We have repeated the calculations of these GBs in graphene with the same type of supercell as h-BN to facilitate direct comparison of energetics. Similar to h-BN, there are two GBs: one at the edge and another at the center of the supercell (chain of rhombii). However, they evolve differently upon structural relaxation. The GB at the center of the graphene supercell evolves into a GB with a set of 2 irregular pentagonal rings with apex angles, 112° and an irregular octagonal ring (Fig. 3a) *i.e.*, the 5:5:8 GB. Interestingly at the boundary of the supercell, we

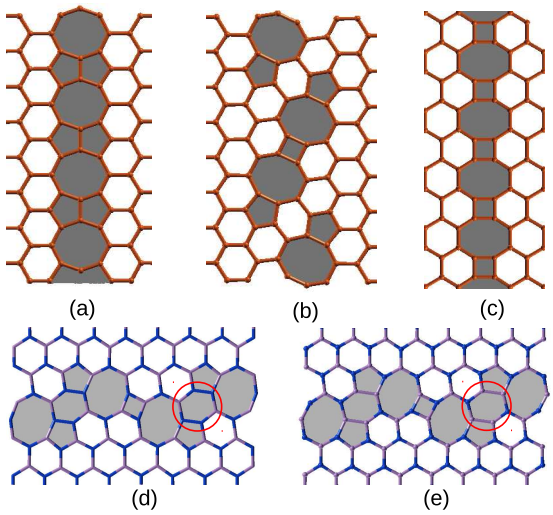


**Fig. 3** Different GBs in graphene and h-BN (a) Structure of 5:5:8 GB in graphene. (a chain of a set of 2 pentagon and octagon falls along the GB) (b) Structure of 6:5:8:4:8:5 GB in graphene ( two set o f one pentagon and octagon oriented oppositely are connected by a rectangle along the GB). (c) Structure of 4:8 GB in graphene (a chain of a set of 1 octagon and rectangle). (d) Structure of 6:5:8:4:8:5 N-N GB in h-BN (two set of one pentagon and octagon oppositely are connected by a rhombus along the GB). (e) Structure of 6:5:8:4:8:5 B-B GB in h-BN (two set of one pentagon and octagon oppositely are connected by a rhombus along the GB). Note that in 6:5:8:4:8:5 N-N and 6:5:8:4:8:5 B-B two set of 5-8-4-8-5 polygons are connected by a distorted hexagon whose opposite sides are B-B/N-N as highlighted in (d) and (e) by red circle. GBs are shown by shadows. Boron (B) atoms are shown in pink and nitrogen (N) in blue.

find a new type of GB with two oppositely oriented pentagon-octagon pairs linked with a rectangular ring (Fig. 3b). This GB is named as the '6:5:8:4:8:5' GB, in which we get irregular pentagonal ring with apex angle 109° and irregular octagonal ring. The energies of 5:5:8 and 6:5:8:4:8:5 GBs (using simulations of ribbon) are 0.52 eV/Å and 0.73 eV/Å respectively (we note that these estimates of energies include the energy cost associated with dangling bonds formed at edge of ribbon). We find that the 5:5:8 GB is lower in energy than the 6:5:8:4:8:5 GB indicating its greater stability in graphene. Our analysis also shows that the 5:5:8 GB is more stable in graphene than h-BN (see Table 1). The reason for this is the extra energy required for the formation of homo-elemental bonds at the GB in h-BN. We explored the feasibility of 6:5:8:4:8:5 GB in h-


This journal is © The Royal Society of Chemistry [year]

Physical Chemistry Chemical Physics Accepted Manuscript

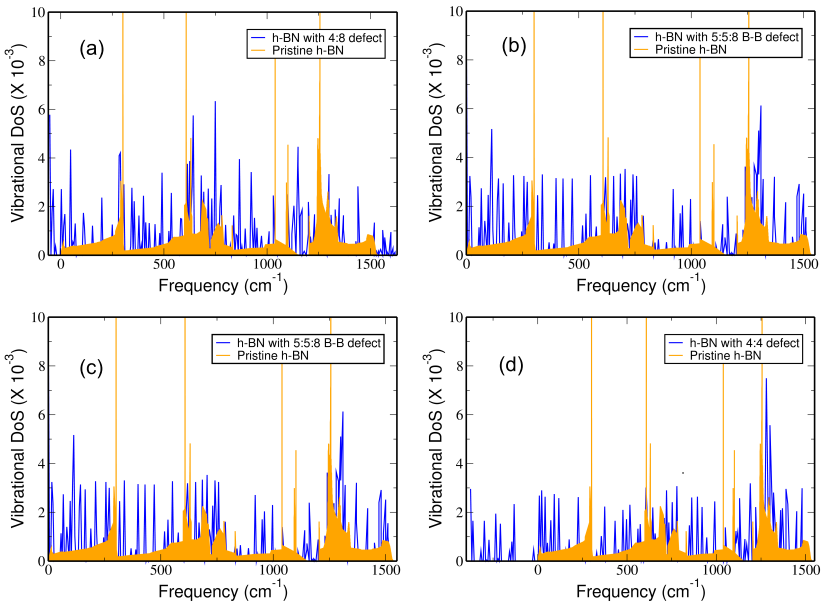


**Fig. 4** Vibrational density of states (Vdos) of perfect BN and BN with GBs. (a) Vdos of pristine and h-BN with 4:8 GB. (b) Vdos of pristine and h-BN with 5:5:8 B-B GB. (c) Vdos of pristine and h-BN with 5:5:8 N-N GB. (d) Vdos of pristine and h-BN with 4:4 GB. Light brown (orange) and blue denote the phonon density of states for pristine h-BN and h-BN with GB respectively.

BN and found two new types of GB structures (6:5:8:4:8:5 B-B and 6:5:8:4:8:5 N-N). The structures of these GBs involve a pair of pentagons and an octagon oppositely oriented, connected by a rhombus and two sets of 5-8-4-8-5 polygons that are connected by a deformed hexagon with B-B/N-N bonds at the opposite sides (see Fig. 3d and e). The energies of 6:5:8:4:8:5 B-B and 6:5:8:4:8:5 N-N GBs are 0.79 eV/Å and 1.10 eV/Å respectively, comparable to energy of other interfaces.

**Table 1** Energies for different grain boundaries (4:8, 5:5:8, 4:4 and 6:5:8:4:8:5 GBs) in h-BN and graphene

| Type of GBs | System | Energy (eV/Å) |
|---|---|---|
| 4:8 | h-BN | 0.48 |
| 4:8 | graphene | 0.74 |
| 5:5:8 N-N | h-BN | 0.77 |
| 5:5:8 B-B | h-BN | 0.65 |
| 4:4* | h-BN | 1.87 |
| 6:5:8:4:8:5 N-N* | h-BN | 1.10 |
| 6:5:8:4:8:5 B-B* | h-BN | 0.79 |
| 5:5:8 | graphene | 0.52 |
| 6:5:8:4:8:5* | graphene | 0.73 |

*novel GBs

### 3.1.3 Relative stability of faults or grain boundaries.

We now discuss the relative stability of GBs in h-BN and graphene, by comparing the energies of the same GB in these materials. It is clear from our results (Table 1) that 4:8 GB (stacking fault) is more stable in h-BN (Fig. 1d) than in graphene (Fig. 3c), and it has the lowest energy, due to formation of the hetero-polar bond at the GB in h-BN. In contrast, a growth fault (5:5:8 GB) is the most stable GB in graphene with energy 0.52 eV/Å. Similarly, the 5:5:8 B-B GB (growth fault) is the most stable GB among all the growth faults in h-BN studied here. While studying growth and stacking faults in h-BN and graphene, we find four new GBs, which have not been reported yet. The 6:8:5:4:8:5 GB in graphene has an energy of 0.73 eV/Å, whereas 4:4, 6:8:5:4:8:5 B-B and 6:8:5:4:8:5 N-N GBs in h-BN have energies of 1.87 eV/Å, 0.79 eV/Å and 1.10 eV/Å respectively. The 6:8:5:4:8:5 GB is energetically more stable in graphene than in h-BN, and 6:8:5:4:8:5 B-B is more stable than the other two GBs in h-BN (6:8:5:4:8:5 B-B and 6:8:5:4:8:5 N-N). The 4:4 GB is relatively higher in energy than any other GB in h-BN, suggesting low likelihood of its occurrence.

## 3.2 Structural instabilities

Structural stability can be affirmed by showing that the structure is a local minimum of energy w.r.t. all structural distortions. To this end, we determine long wavelength phonons of

Physical Chemistry Chemical Physics Accepted Manuscript

the supercell (at Γ-point). Vibrational density of states (Fig. 4) of h-BN with 4:8, 4:4 and 5:5:8 N-N GBs, reveal the presence of unstable modes (*i.e.* imaginary frequencies), whereas 5:5:8 B-B does not have any unstable modes, implying the structure of h-BN with 5:5:8 B-B GB is stable, *i.e.* local minimum of energy. On the other hand, these unstable modes conclusively show that the structure is not a local minimum of energy, but is a saddle point. Eigen-modes of phonons with imaginary frequencies in the vibrational spectrum of defective h-BN involve atomic displacements that lead to out-of-plane deformation along these interfaces (see Fig. 5a, b and 6a, b).

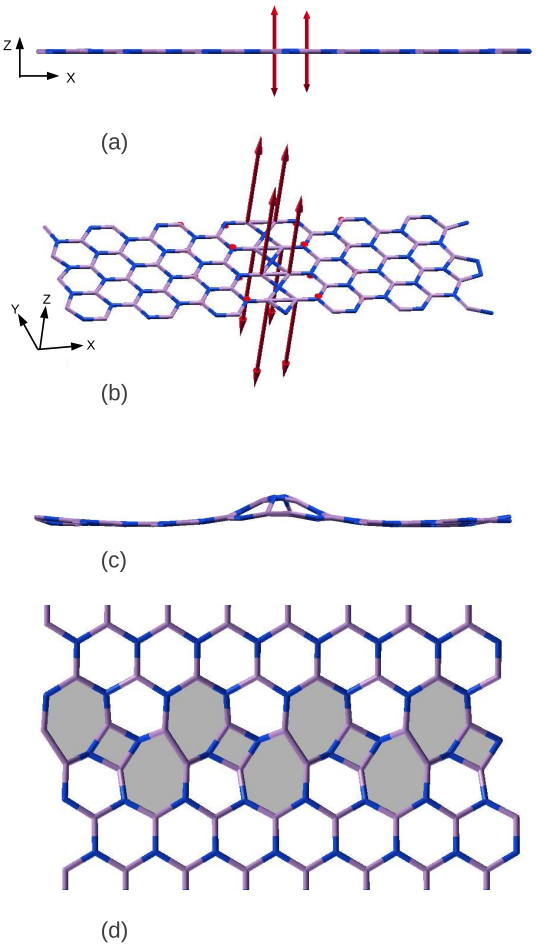


**Fig. 5** Phonon modes constituting the structural instability of h-BN with 4:4 GB (a), (b) Two views of atomic displacements of the mode with a frequency ≈375i cm$^{-1}$ (wave like deformat ion at GB). (c) Freezing in the same mode leads to buckling of the sheet which is centered at GB (side view of the sheet). (d) Top view of 4:4 GB (which evolves on relaxation), which has two heptagons sharing a B-B bond side connected with a rhombus. Boron (B) atoms are shown in pink and nitrogen (N) in blue.

We distort the structure by freezing in small atomic displacements corresponding to eigen modes of the lowest energy unstable modes (strongest instability) (which are 53 cm$^{-1}$, 375 cm$^{-1}$ and 40 cm$^{-1}$ for 4:8, 4:4 and 5:5:8 N-N GBs respectively). The unstable modes of 4:8 and 4:4 GBs have oscillatory deformation localized (like a wave) along the GB (Fig. 5a, b and Fig. 6a, b), whereas the unstable mode of 5:5:8 N-N has deformation wave running along the edge of the ribbon (not at the GB) (see Fig. 6c and d).

In the 4:4 GB, N-atom is coordinated with four boron atoms through sp$^3$ bonding, hence it tries to deviate from planar to tetrahedral structure. A set of two B-atoms placed opposite to N atom tries to move in opposite direction to achieve tetrahedral structure (see Fig. 5b). Upon structural relaxation, the h-BN sheet with these GBs buckle, *i.e.*, becomes non-planar. Such buckling of the sheet reduces the energy of 4:8 GB by 19.5%. For this GB, the rippling amplitude (the difference along the z-axis of the highest and lowest atom) is ∼ 0.35 Å, which is quite sizable and should be readily observable. There is not a considerable change in energy of 5:5:8 N-N GB due to buckling even though its rippled structure has an amplitude of 0.42 Å, suggesting a rather flat energy landscape of rippling. Structural relaxation of h-BN with a 4:4 GB after freezing in the displacements of lowest energy unstable mode, lowers its energy by 39.5%. The resulting structure exhibits a wrinkle (short length-scale deformation) at the interface (Fig. 5b). Its structure (a chain of rhombii) evolves to a completely different structure (a chain of two heptagons and a rhombus). In this transformed structure, the two heptagons share a B-B bond as one of its sides (Fig. 5d) and the rippling amplitude (1.6 Å) is quite significant. This deformation structure involving large displacement of most of the atoms at the GB constitute a wrinkle (see Fig. 5c). Liu *et. al*[33] have studied similar defect as 4:8 GB, but missed the deviation from planarity of asym-0° (120° and 240°)[33] GBs (4:8 GB in our case). In contrast we find that h-BN with a 4:8 GB does show buckling and there is noticeable reduction in energy by huge amount (19.5%).

### 3.3 Vibrational and electronic signatures

**3.3.1 Vibrational signatures.** The structural changes associated with these interfaces in h-BN are responsible for the changes in vibrational spectra, which can be identified in Raman and IR spectra. The unit cell of 2-D h-BN contains two atoms, and belongs to the point group $D_{3h}$ and space group ($P\bar{6}2m$). Its optical phonon modes are categorized into $A_2'' + 2E'$ modes, where mode $A_2''$ is IR active and an $E'$ mode is both IR and Raman active ($E'$ is a doubly degenerate in-plane bond stretching mode).[43] Our estimates of frequencies of $A_2''$ and $E'$ modes are 791 cm$^{-1}$ and 1382 cm$^{-1}$ respectively, which agree well (within 1%) with experimental values reported earlier.[44] The frequency and eigen displacement of $A_2''$


This journal is © The Royal Society of Chemistry [year]

Physical Chemistry Chemical Physics Accepted Manuscript

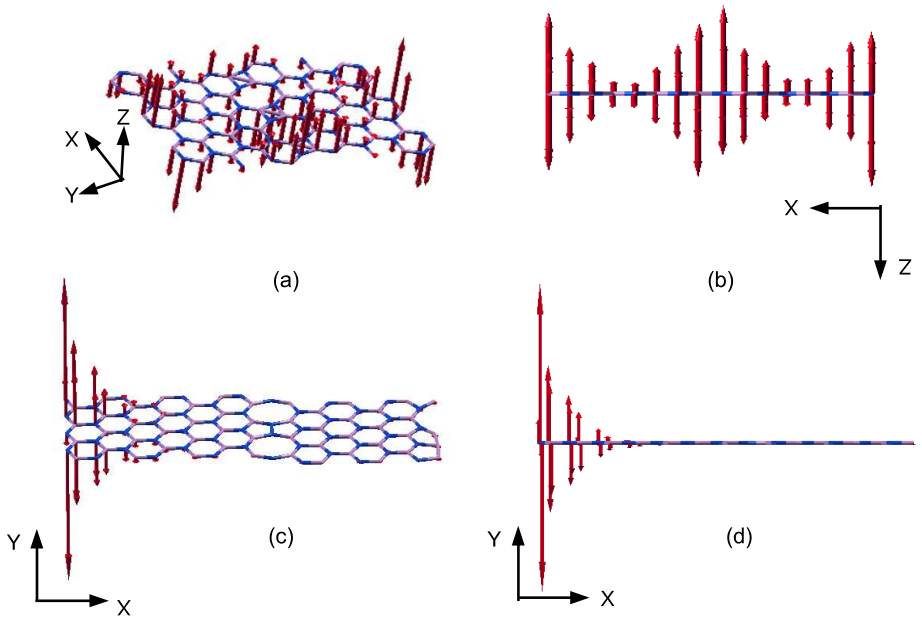


**Fig. 6** Phonon mode which constitutes the structural instability of h-BN with 4:8 GB, two views of atomic displacements of the mode with a frequency ≈53i cm$^{-1}$ (wave propagates along th e GB) as shown (a) and (b). Phonon modes constitutes the structural instability of h-BN with 5:5:8 N-N GB, two views of atomic displacements of the mode with a frequency ≈40i cm$^{-1}$ as shown in (c) and (d). Boron (B) atoms are shown in pink and nitrogen (N) in blue.

and $E'$ modes are modified by these interfaces, due to structural modifications at their GB. To identify $A_2''$ and $E'$ modes of the h-BN supercell with a 4:8 GB, we project its normal modes ($e'_\nu$) onto those of pristine h-BN ($e_\mu$), by calculating an overlap matrix ($S_{\mu\nu}$) given by,

$$S_{\mu\nu} = \langle e_\mu | e'_\nu \rangle \quad (2)$$

The $A_2''$ and $E'$ modes of the defective h-BN are identified as those having the largest overlap ($|S_{\mu\nu}|$) with the $A_2''$ and $E'$ eigenvectors of pristine h-BN.

Due to the GB, the symmetry equivalence between $x$ and $y$ directions in the hexagonal lattice is broken, and hence the degeneracy of $E'$ mode is lifted. The $A_2''$ mode softens by 14 cm$^{-1}$, 10 cm$^{-1}$ and 14 cm$^{-1}$ due to 4:8 , 5:5:8 N-N and 4:4 GBs respectively (see Table 2). In presence of 5:5:8 B-B GB, the $A_2''$ mode hardens by 38 cm$^{-1}$. The $E'$ mode softens by 21 cm$^{-1}$ and 25 cm$^{-1}$, and hardens by 5 cm$^{-1}$ and 10 cm$^{-1}$ due to 5:5:8 N-N, 5:5:8 B-B, 4:8 and 4:4 GBs respectively for the vibration (in xy-plane) along the GB. The another in-plane $E'$ mode softens by 26 cm$^{-1}$ and 3 cm$^{-1}$ (not significant) and hardens by 12 cm$^{-1}$ and 106 cm$^{-1}$ (significant) for 5:5:8 N-N, 4:4, 4:8 and 5:5:8 B-B GBs respectively for vibrations in the xy-plane involving displacements perpendicular to the GB (refer Table 2). Such shifts in frequencies can be observed experimentally with IR and Raman spectroscopies. The softening (hardening) of these modes is readily understood in terms of stretching (contraction) of the in-plane (out-of-plane) bonds.

**3.3.2 Electronic signatures.** We now identify electronic signatures of the lowest energy GB (4:8 GB) in h-BN through comparison with pristine h-BN. Its electronic density of states (DoS) reveals two extra peaks (Fig. 7a) at the valence band maximum (VBM) and the conduction band minimum (CBM). Further analysis of the charge density of these states indicates that these electronic states are localized at the GBs, confirming these extra peaks constitute characteristic signatures of the 4:8

Physical Chemistry Chemical Physics Accepted Manuscript

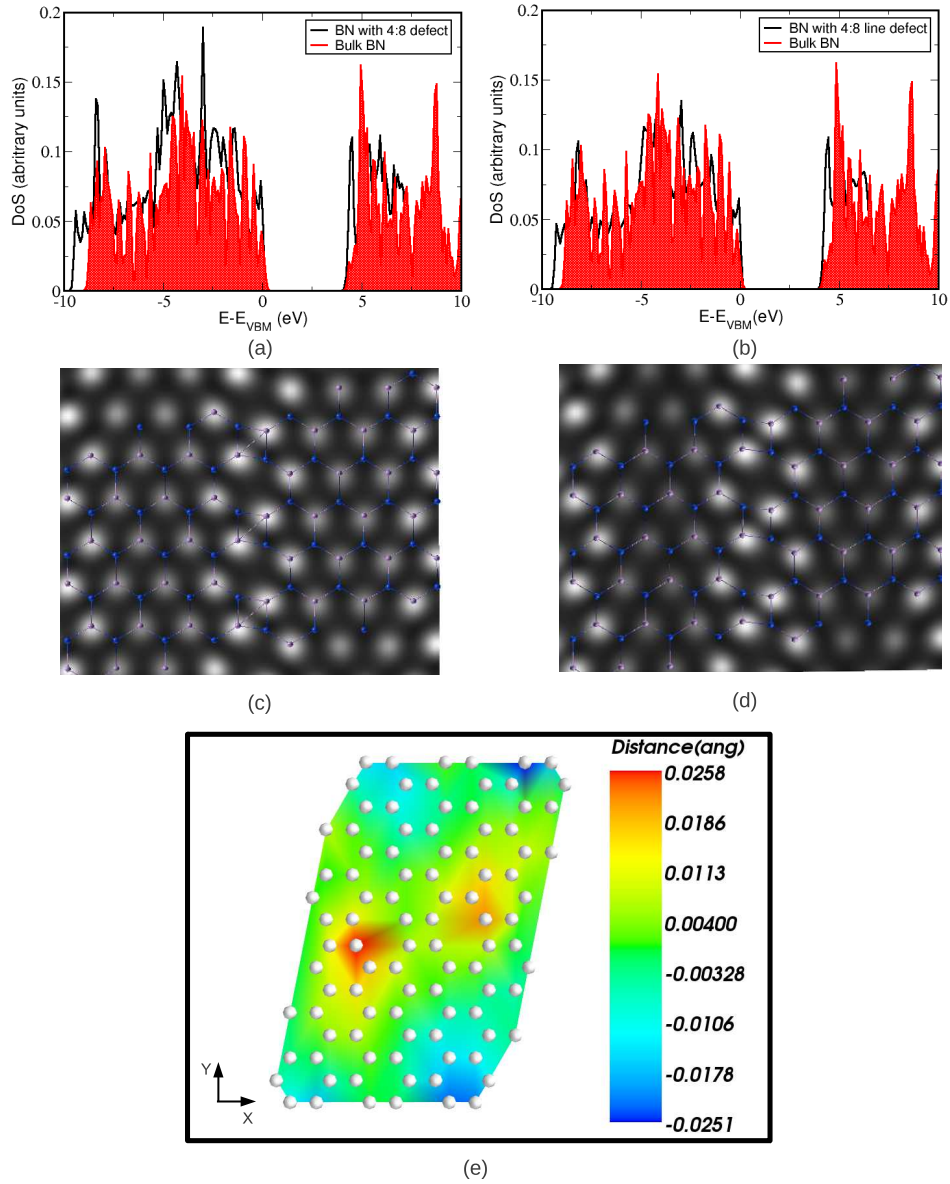


**Fig. 7** Electronic signature of 4:8 GB in h-BN seen in the density of states of (a) planar and (b) buckled (i.e. non-planar) structures (compared with pure h-BN). Atomic structures juxtaposed on simulated STM images of planar (c) and non-planar (d) h-BN with 4:8 GB. (g) Buckled h-BN sheet with different colors showing the extent to which different atoms displace out of plane.

GB. From the comparison of the electronic DoS of planar and non-planar GB structures, a few extra peaks are evident in the DoS of the non-planar structure, indicating a redistribution of localized electronic states upon buckling.

To facilitate experimental observations and verification, we obtain simulated scanning tunneling microscopy (STM)[45] images. They were obtained keeping the tip at a constant height of 1Å above the surface of h-BN with a positive sample bias of 0.8V with respect to the CBM. For a positive sample bias, induced charge accumulation is observed at B atoms whose orbitals constitute the conduction band. Simulated STM images (Fig. 7c and d) highlight the difference between electronic structure of the planar and non-planar structures of the defective h-BN. We notice that the bright features in the bulk planar structure weaken upon buckling (clear from the STM image of the non-planar structure), showing that charge accumulation remains localized at the GB even after buckling.


This journal is © The Royal Society of Chemistry [year]

Physical Chemistry Chemical Physics Accepted Manuscript

**Table 2** Vibrational spectroscopic signatures in the Raman and IR active modes of h-BN with different GBs (4:8, 5:5:8, 4:4) and shifts in frequencies ($\Delta\omega$ in $cm^{-1}$) w.r.t. pristine h-BN

| Pristine (h-BN) ($cm^{-1}$) | h-BN with 4:8 GB ($cm^{-1}$) | h-BN with 5:5:8 B-B GB ($cm^{-1}$) | h-BN with 5:5:8 N-N GB ($cm^{-1}$) | h-BN with 4:4 GB ($cm^{-1}$) |
|---|---|---|---|---|
| 791 (IR active) | 777 ($\Delta\omega$= -14) | 829 ($\Delta\omega$= +38) | 781 ($\Delta\omega$= -10) | 778 ($\Delta\omega$= -14) |
| 1382 (Raman and IR active) | 1389 ($\Delta\omega$= +5) | 1392 ($\Delta\omega$= +10) | 1361 ($\Delta\omega$= -21) | 1357 ($\Delta\omega$= -25) |
| 1382 (Raman and IR active) | 1394 ($\Delta\omega$= +12) | 1379 ($\Delta\omega$= -3) | 1356 ($\Delta\omega$= -26) | 1488 ($\Delta\omega$= +106) |

## 4 Conclusions

We presented a comparative analysis of changes in the structure and vibrational properties associated with two types of interfaces categorized into: (i) stacking and (ii) growth faults in h-BN and graphene. We demonstrated that a 4:8 GB (stacking fault) is more stable in h-BN, while a 5:5:8 GB (growth fault) is relatively more stable in graphene. We reported four new types of GBs: 6:5:8:4:8:5 GB in graphene and 4:4, 6:5:8:4:8:5 N-N and 6:5:8:4:8:5 B-B GBs in h-BN. The 6:5:8:4:8:5 GB in graphene, which is not reported so far, has the lowest energy among all the four GBs, and should therefore be common and relevant to experiment. Our work highlights the remarkable diversity in the structures of grain boundaries even when the angle between the grains is fixed at 60°.

Furthermore, our analysis of the lattice dynamical (phonon) spectrum of the planar structure with these GBs (4:8, 5:5:8 N-N and 4:8) revealed unstable modes, *i.e*. structural instabilities with respect to buckling initiated at the interface. These lead to formation of wrinkles (short length scale buckling) at the interfaces and associated rippling (long length scale buckling) of the structure, which are relevant to the evolution of nanoforms to 3-D frameworks. Vibrational signatures identified here, specifically hardening and softening (frequency shifts) of $A_2''$ and $E'$ modes, will be useful in characterization of these interfaces with IR and Raman spectroscopies. Electronic signature of the lowest energy 4:8 GB of h-BN is identified in the additional peaks at the VBM and the CBM that are associated with charge accumulation localized at the interface, and is accessible to STM.

## Acknowledgement

The authors are thankful to the Centre for Computational Materials Science (CCMS) at Jawaharlal Nehru Centre for Advanced Scientific Research (JNCASR) for providing computational facilities.A.S. is thankful to JNCASR, India, for a Research Fellowship. UVW acknowledges support from a J. C. Bose National Fellowship of the Department of Science and Technology (India).

## References

1 H. W. Kroto, J. R. Heath, S. C. O'Brien, R. F. Curl and R. E. Smalley, *Nature*, 1985, **318**, 162–163.
2 S. Iijima, *Nature*, 1991, **354**, 56–58.
3 A. K. Geim and K. S. Novoselov, *Nat. Mater.*, 2007, **6**, 183–191.
4 Z. Chen, Y. Yuan, H. Zhou, X. Wang, Z. Gan, F. Wang and Y. Lu, *Advanced Materials*, 2014, **26**, 339–345.
5 H. Jiang, P. S. Lee and C. Li, *Energy Environ. Sci.*, 2013, **6**, 41–53.
6 L. S. Panchakarla, K. S. Subrahmanyam, S. K. Saha, A. Govindaraj, H. R. Krishnamurthy, U. V. Waghmare and C. N. R. Rao, *Advanced Materials*, 2009, **21**, 4726–4730.
7 D. P. Hashim, N. T. Narayanan, J. M. Romo-Herrera, D. A. Cullen, M. G. Hahm, P. Lezzi, J. R. Suttle, D. Kelkhoff, E. Muñoz Sandoval, S. Ganguli, A. K. Roy, D. J. Smith, R. Vajtai, B. G. Sumpter, V. Meunier, H. Terrones, M. Terrones and P. M. Ajayan, *Sci. Rep.*, 2012, **2**, 363.
8 A. Stone and D. Wales, *Chemical Physics Letters*, 1986, **128**, 501 – 503.
9 X. Li, X. Wu, X. C. Zeng and J. Yang, *ACS Nano*, 2012, **6**, 4104–4112.
10 S. Stankovich, D. A. Dikin, R. D. Piner, K. A. Kohlhaas, A. Kleinhammes, Y. Jia, Y. Wu, S. T. Nguyen and R. S. Ruoff, *Carbon*, 2007, **45**, 1558 – 1565.
11 Y. Shi, C. Hamsen, X. Jia, K. K. Kim, A. Reina, M. Hofmann, A. L. Hsu, K. Zhang, H. Li, Z.-Y. Juang, M. S. Dresselhaus, L.-J. Li and J. Kong, *Nano Lett.*, 2010, **10**, 4134–4139.
12 Y. Si and E. T. Samulski, *Nano Lett.*, 2008, **8**, 1679–1682.
13 K. K. Kim, A. Hsu, X. Jia, S. M. Kim, Y. Shi, M. Hofmann, D. Nezich, J. F. Rodriguez-Nieva, M. Dresselhaus, T. Palacios and J. Kong, *Nano Lett.*, 2012, **12**, 161–166.
14 S. J. Chae, F. Güneş, K. K. Kim, E. S. Kim, G. H. Han, S. M. Kim, H.-J. Shin, S.-M. Yoon, J.-Y. Choi, M. H. Park, C. W. Yang, D. Pribat and Y. H. Lee, *Advanced Materials*, 2009, **21**, 2328–2333.
15 W. Auäwter, H. U. Suter, H. Sachdev and T. Greber, *Chemistry of Materials*, 2004, **16**, 343–345.
16 J. C. Meyer, C. Kisielowski, R. Erni, M. D. Rossell, M. F. Crommie and A. Zettl, *Nano Lett.*, 2008, **8**, 3582–3586.
17 A. Nag, K. Raidongia, K. P. S. S. Hembram, R. Datta, U. V. Waghmare and C. N. R. Rao, *ACS Nano*, 2010, **4**, 1539–1544.
18 C. Jin, F. Lin, K. Suenaga and S. Iijima, *Phys. Rev. Lett.*, 2009, **102**, 195505.
19 P. Y. Huang, C. S. Ruiz-Vargas, A. M. van der Zande, W. S. Whitney, M. P. Levendorf, J. W. Kevek, S. Garg, J. S. Alden, C. J. Hustedt, Y. Zhu, J. Park, P. L. McEuen and D. A. Muller, *Nature*, 2011, **469**, 389–392.
20 A. Zobelli, C. P. Ewels, A. Gloter, G. Seifert, O. Stephan, S. Csillag and C. Colliex, *Nano Lett.*, 2006, **6**, 1955–1960.
21 M. U. Kahaly, S. P. Singh and U. V. Waghmare, *Small*, 2008, **4**, 2209–2213.
22 S. N. Shirodkar and U. V. Waghmare, *Phys. Rev. B*, 2012, **86**, 165401.
23 S. Bhowmick and U. V. Waghmare, *Phys. Rev. B*, 2010, **81**, 155416.
24 J. Červenka and C. F. J. Flipse, *Phys. Rev. B*, 2009, **79**, 195429.

Physical Chemistry Chemical Physics Accepted Manuscript

25 N. M. R. Peres, F. Guinea and A. H. Castro Neto, *Phys. Rev. B*, 2006, **73**, 125411.
26 O. V. Yazyev and S. G. Louie, *Nat. Mater.*, 2010, **9**, 806–809.
27 A. Mesaros, S. Papanikolaou, C. F. J. Flipse, D. Sadri and J. Zaanen, *Phys. Rev. B*, 2010, **82**, 205119.
28 Y. Liu and B. I. Yakobson, *Nano Lett.*, 2010, **10**, 2178–2183.
29 R. Grantab, V. B. Shenoy and R. S. Ruoff, *Science*, 2010, **330**, 946–948.
30 S. Malola, H. Häkkinen and P. Koskinen, *Phys. Rev. B*, 2010, **81**, 165447.
31 J. Cervenka, M. I. Katsnelson and C. F. J. Flipse, *Nat Phys*, 2009, **5**, 840–844.
32 H. F. Bettinger, T. Dumitrică, G. E. Scuseria and B. I. Yakobson, *Phys. Rev. B*, (2002), **65**, 041406.
33 Y. Liu, X. Zou and B. I. Yakobson, *ACS Nano*, 2012, **6**, 7053–7058.
34 O. V. Yazyev and S. G. Louie, *Phys. Rev. B*, 2010, **81**, 195420.
35 J. M. Carlsson, L. M. Ghiringhelli and A. Fasolino, *Phys. Rev. B*, 2011, **84**, 165423.
36 T.-H. Liu, G. Gajewski, C.-W. Pao and C.-C. Chang, *Carbon*, 2011, **49**, 2306 – 2317.
37 W. Zhou, X. Zou, S. Najmaei, Z. Liu, Y. Shi, J. Kong, J. Lou, P. M. Ajayan, B. I. Yakobson and J.-C. Idrobo, *Nano Lett.*, 2013, **13**, 2615–2622.
38 J. E. Northrup, J. Neugebauer and L. T. Romano, *Phys. Rev. Lett.*, 1996, **77**, 103–106.
39 P. Giannozzi, S. Baroni, N. Bonini, M. Calandra, R. Car, C. Cavazzoni, D. Ceresoli, G. L. Chiarotti, M. Cococcioni, I. Dabo, A. D. Corso, S. de Gironcoli, S. Fabris, G. Fratesi, R. Gebauer, U. Gerstmann, C. Gougoussis, A. Kokalj, M. Lazzeri, L. Martin-Samos, N. Marzari, F. Mauri, R. Mazzarello, S. Paolini, A. Pasquarello, L. Paulatto, C. Sbraccia, S. Scandolo, G. Sclauzero, A. P. Seitsonen, A. Smogunov, P. Umari and R. M. Wentzcovitch, *J. Phys: Condens. Matter*, 2009, **21**, 395502.
40 J. P. Perdew, K. Burke and M. Ernzerhof, *Phys. Rev. Lett.*, 1996, **77**, 3865–3868.
41 D. Vanderbilt, *Phys. Rev. B*, 1990, **41**, 7892–7895.
42 M. S. C. Mazzoni, R. W. Nunes, S. Azevedo and H. Chacham, *Phys. Rev. B*, 2006, **73**, 073108.
43 M. Topsakal, E. Aktürk and S. Ciraci, *Phys. Rev. B*, 2009, **79**, 115442.
44 R. Geick, C. H. Perry and G. Rupprecht, *Phys. Rev.*, 1966, **146**, 543–547.
45 J. Tersoff and D. R. Hamann, *Phys. Rev. B*, 1985, **31**, 805–813.


Physical Chemistry Chemical Physics Accepted Manuscript


This journal is © The Royal Society of Chemistry [year]

## Table of content:

We present new type of grain boundaries in h-BN and graphene, and demonstrate associated wrinkle formation buckling instability.

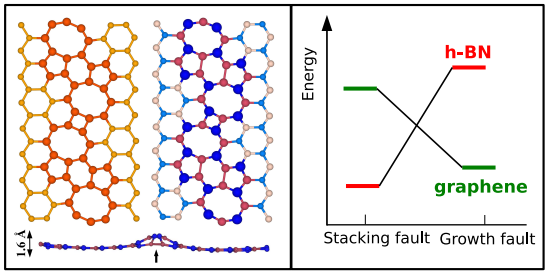


Physical Chemistry Chemical Physics Accepted Manuscript

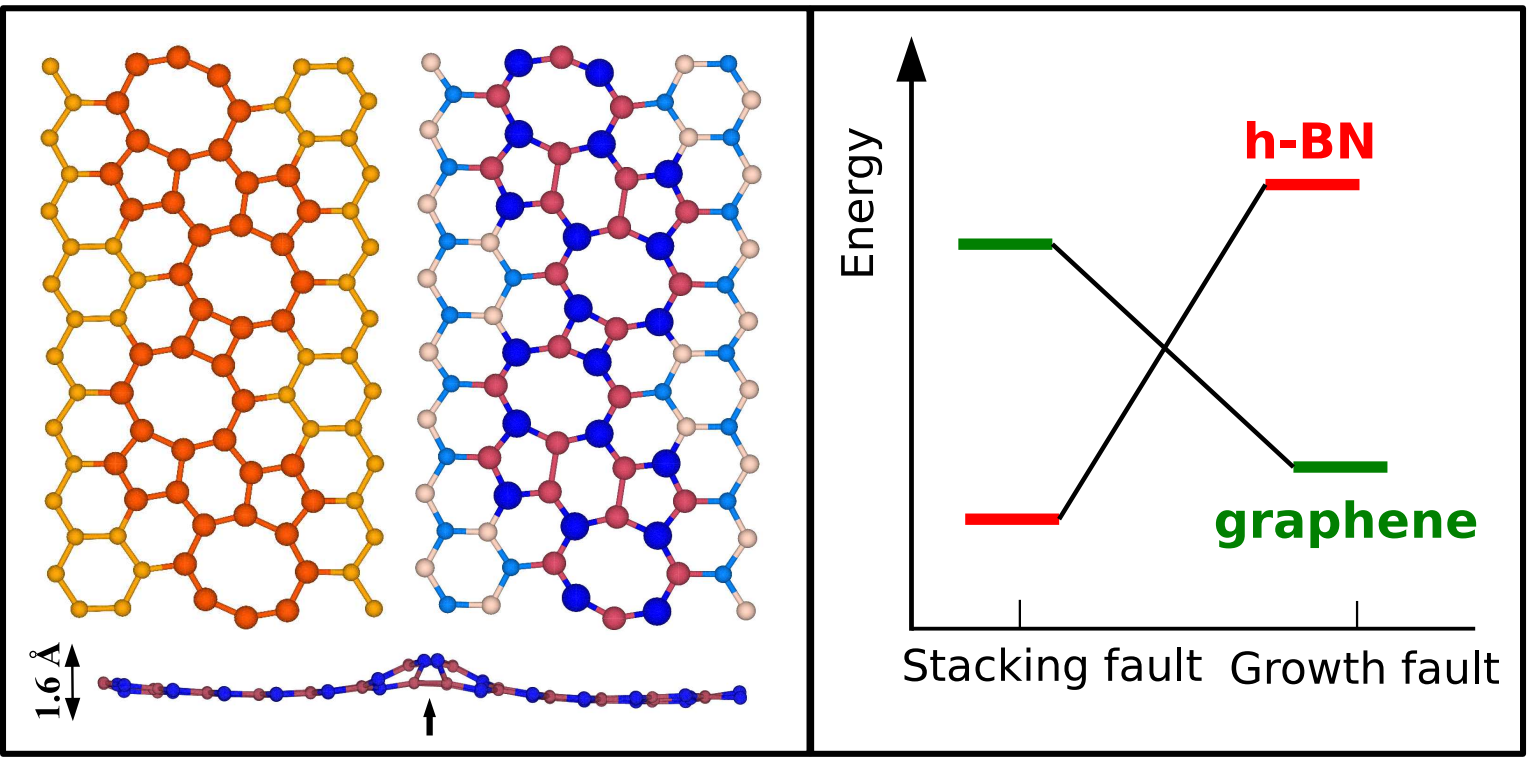


Physical Chemistry Chemical Physics Accepted Manuscript